Quantitative Myocardial Perfusion with 2D and 3D Sequences Alternating Every Heartbeat

Qi Huang
U of U: University of Utah https://orcid.org/0000-0001-6545-2487
Ye Tian
University of Southern California
Jason Mendes
University of Utah Health
Ravi Ranjan
University of Utah Health
Ganesh Adluru
University of Utah Health
Edward DiBella (edward.dibella@hsc.utah.edu)
University of Utah Health https://orcid.org/0000-0001-9196-3731

Research Article

Keywords: Myocardial perfusion, SMS, Stack-of-Stars, Quantitative myocardial blood flow

Posted Date: December 6th, 2021

DOI: https://doi.org/10.21203/rs.3.rs-1129452/v1

Abstract

Purpose

To evaluate a myocardial perfusion acquisition that alternates 2D simultaneous multi-slice (SMS) and 3D stack-of-stars (SoS) acquisitions each heartbeat.

Methods

A hybrid saturation recovery radial 2D SMS and a saturation recovery 3D SoS sequence were created for the quantification of myocardial blood flow (MBF). Initial studies were done to study the effects of using only every other beat for the 2D SMS in two subjects, and for the 3D SoS in two subjects. Alternating heartbeat 2D SMS and 3D SoS were then performed in ten dog studies at rest, four dog studies at adenosine stress, and two human resting studies. 2D SMS acquisition acquired three slices and 3D SoS acquired six slices. An arterial input function (AIF) for 2D SMS was obtained using the first 24 rays. For 3D, the AIF was obtained in a 2D slice prior to each 3D SoS readout. Quantitative MBF analysis was performed for 2D SMS and 3D SoS separately, using a two-compartment model.

Results

Acquiring every-other-beat data resulted in 5-20% perfusion changes at rest for both 2D SMS and 3D SoS methods. For alternating acquisitions, 2D SMS and 3D SoS quantitative perfusion values were comparable for both the twelve rest studies (2D SMS: 0.68±0.15 vs 3D: 0.69±0.15 ml/g/min, p=0.85) and the four stress studies (2D SMS: 1.28±0.22 vs 3D: 1.30±0.24 ml/g/min, p=0.66).

Conclusion

Every-other-beat acquisition changed estimated perfusion values relatively little for both sequences. 2D SMS and 3D SoS gave similar quantitative perfusion estimates when used in an alternating every-other-heartbeat acquisition. Such an approach allows consideration of more diverse perfusion acquisitions that could have complementary features, although testing in a cardiac disease population is needed.

1. Introduction

First-pass myocardial perfusion MRI with gadolinium contrast is an important imaging test for coronary artery disease. After intravenous injection of gadolinium contrast agent, multiple T1-weighted images are acquired each heartbeat. These images are commonly used for qualitative assessment of myocardial perfusion since regional signal differences and delays in the enhancement in the heart are often indicative of regional ischemia [1, 2]. However, poor spatial resolution of the images and artifacts such as dark rim can limit the accuracy of qualitative assessment. Quantitative analysis of first-pass myocardial perfusion imaging may detect regional defects more accurately [3–5]. The performance of both qualitative and quantitative approaches is highly dependent on the use of robust and reliable pulse sequences.

Compared to conventional 2D perfusion sequences, 2D SMS or 3D perfusion MRI imaging sequences may provide more heart coverage or faster image acquisition [6–8]. SMS imaging uses multiple slice-selective RF pulses combined with parallel imaging and phase modulation methods (controlled aliasing in parallel imaging results in higher acceleration (CAIPIRINHA)) to enable acquisitions and reconstruction of several separate slices simultaneously without a cost of spatial or temporal resolution [9–14]. Compared to conventional sequential multi-slice imaging, SMS imaging has the advantage of a short total acquisition time and the possibility of whole-heart coverage by using multiple slice groups [15]. While acquisitions with up to five simultaneously acquired slices (multi-band factor of 5, MB=5) for cardiac perfusion have been reported, a degradation of image quality was seen compared to the image quality obtained with a multi-band factor of 2 or 3 [16]. Both radial and spiral acquisitions have demonstrated the feasibility of acquiring multiple SMS sets with a high MB factor at heartrates up to 100 beats per minute or higher[17, 18]. Using MB=3, nine slices can be acquired each heartbeat at heartrates below 100 beats per minute. However, only a few studies on the quantification of 2D SMS myocardial perfusion imaging have been published [19, 20].

High SNR and whole heart coverage can be achieved with 3D imaging [6]. However, the 3D readout must be done quickly, while the heart is relatively still. Recent developments in reconstruction with undersampled data have improved the temporal fidelity to ~200 ms readouts and have increased the spatial resolution of 3D myocardial perfusion images at high accelerations [21–28]. For example, multi-coil and k-t principal component analysis reconstruction method have been used to provide 3D myocardial perfusion images with a spatial resolution of 2 mm [29]. A shorter total readout time of 150 ms has also been reported [30]. Quantitative 3D myocardial perfusion studies have been shown to be feasible if an accurate AIF is acquired [30]. Furthermore, 3D quantitative analysis with myocardial perfusion reserve (MPR) yielded high diagnostic accuracies in both systole and diastole, comparable with previous 2D studies [28, 31, 32].

Acquisitions with 2D SMS and 3D methods have trade-offs in resolution and coverage and image quality [33]. Compared to 2D SMS imaging, the advantages of 3D techniques include increased slice resolution and more tractable respiratory motion due to the coherent motion of all the slices [8]. Regardless of these benefits, the problem of increased acquisition time, greater undersampling factors and the associated decreased spatial resolution [34, 35] have limited 3D methods. Thus, the choice when performing quantitative assessment of myocardial perfusion imaging is unclear - whether 2D SMS or 3D imaging should be selected for specific populations with cardiac disease.

In this study, we propose a new perfusion acquisition that alternates between a radial 2D SMS with a “hybrid” weighting of saturation recovery and steady-state gradient echo signals and a 3D SoS acquisition each heartbeat [36].

2. Methods

Overview

First, to investigate the effects of acquisition every other heartbeat on both the AIF and myocardial signals, five scans using radial 2D SMS and 3D SoS acquisitions were performed every heartbeat. Four of the five scans were analyzed using either only the even or the odd time frames, to understand how well an alternating beat acquisition would perform. Then, an alternating 2D/3D saturation-recovery sequence was implemented, and both phantom and in-vivo data of seven dogs (10 rest and 4 stress studies) and two human subjects were acquired and processed to study the differences and comparable aspects of the 2D SMS and 3D SoS methods.

2.1 Pulse Sequence

All scans were performed at 3T using a Prisma MRI system (Siemens Medical Solutions, Erlangen, Germany).

2.1.1 Every heartbeat acquisition

Both 2D SMS and 3D SoS sequences were performed as separate free-breathing acquisitions with “standard” every-beat ECG-gated acquisitions. The 2D SMS acquisition had a single saturation pulse each beat and then a short 20msec recovery time before using radial RF-spoiled gradient echo readouts. The readouts continued until the next R-wave trigger was detected. A continuous golden angle increment was used for all the rays. One slice group with a multi-band factor of 3 was acquired throughout each heartbeat. There was a slice gap equal to one slice thickness. The 2D SMS acquired ~300 rays per heartbeat (for a heart rate of ~80 beats per minute). The first 24 rays were used to reconstruct images for the AIF. Retrospectively, rays for the reconstruction of the tissue curves were selected as those acquired around systole. This was typically 25-96 rays, starting at approximately ray 40, depending on the heart rate. Selection of rays is detailed in the Reconstruction section below.

A 3D SoS acquisition every beat was also acquired. The pulse sequence consisted of a 2D saturation recovery AIF acquisition followed by a ~200msec 3D SoS acquisition as in [30]. In each beat, the 2D AIF was acquired from 24 rays starting 20msec after a saturation pulse. Then another saturation pulse was performed and after recovery, the 3D readout started. Though a longer saturation recovery time (SRT), typically 150msec, was desired in terms of better contrast, a shorter SRT, like 100msec, was applied due to high heart rates, especially during stress. Scan parameters for 3D SoS: 92 rays each heartbeat, variable density in k_z with 24 rays in the center section and six partitions acquired in total (eight slices reconstructed due to zero-padding in the k-space and center six slices used for analysis).

Saturation pulses as in [37] were used. The main imaging parameters used in 2D SMS and 3D SoS sequences are listed in Table 1.

Table 1: Imaging parameters used in 2D SMS and 3D SoS sequences

Parameters	2D SMS	3D SoS
Repetition time (TR), msec	2.3	2.1
Echo time (TE), msec	1.1	1.1
Flip angle, °	12	12
Flip angle in proton density, °	2	2
Proton Density Frames	10	10
Slice thickness, mm	5-8	5
Saturation recovery time (SRT), msec	20	100
Field of view (FOV), mm^2	260×260	260×260
Matrix size	144×144	144×144
Number of coil channels	30 or 34	20, 30 or 34

2.1.2 Effects of acquisition every other beat on the AIF and myocardial signals

Data acquisitions were obtained in two subjects for 2D SMS and three subjects for 3D SoS, as described next. In these datasets, data with large variance possibly caused from motion were discarded. To be specific, if myocardial tissue signal intensities in two neighboring time frames in a slice of every-beat data differed by more than 20% for 10 consecutive frames, that subject was not analyzed. One 3D subject was left out for this reason, so two 2D SMS and two 3D SoS every-beat datasets were analyzed.

The effect of every-other-beat acquisition was investigated using every-beat data. The analysis was performed by comparison between data with every-beat (EB) acquisition, called the EB group, and using every-other-beat, (the EOB group), in both 2D SMS and 3D SoS subjects. To focus on the undersampling and minimize errors caused by reconstruction and post-processing, an “ideal” scenario was investigated first. That is, the EB data was reconstructed and registered, then divided into two EOB groups (odd and even) equally and processed in the following manner: (1) the same proton density (PD) signal intensities were used for both the EB and the EOB data; (2) the same myocardial region-of-interest (ROI) contours and shift adjustments were applied for both EB and EOB group; (3) gadolinium concentration ([Gd]) curves from the EB group were divided into two EOB sets.

However, actual data with other effects can be more complicated. Respiratory and cardiac motion, for example, might result in larger heart motion displacement between two neighboring image frames in an EOB acquisition compared to that of an EB acquisition. Such motion and fewer time frames relative to EB can reduce the performance of the reconstruction methods that include temporal regularization.

In this work, we included the practical “non-ideal” case, where the reconstruction and the processing of 2D SMS and 3D SoS data in the alternating 2D/3D acquisition were done independently, which is different from the ideal case described above. Thus, EB k-space data was separated into the even and odd EOB groups, and then each group was reconstructed, registered and quantified individually. To reduce variability, the same contour from EB data was applied to EOB data processing. In addition, the same proton density images were also used for EB and EOB data processing.

The overall workflow of acquisition, reconstruction and data processing is shown in Figure 1. The next section details the reconstruction and conversion to [Gd] for quantification of EB and EOB data.

2.2 Reconstruction

Both 2D SMS and 3D SoS datasets were reconstructed by a joint spatial and temporal constrained reconstruction (STCR) method [16, 38, 39]. The STCR reconstruction minimized a cost function that consisted of an L2 data fidelity term between the estimated image and the undersampled data and L1 terms of spatial and temporal total variations (TV) as in equation (1). Pre-interpolation with GRAPPA operator gridding (GROG) was used to convert the radial sampling data onto a Cartesian grid as an initial step [40]. The cost function used for the 3D SoS data reconstruction is:

$$C = \|WFSm - d\|_2^2 + \alpha_{xy} \left\| \sqrt{(\nabla_x m)^2 + (\nabla_y m)^2 + \varepsilon} \right\|_1 + \alpha_t \left\| \sqrt{(\nabla_t m)^2 + \varepsilon} \right\|_1 + \alpha_z \left\| \sqrt{(\nabla_z m)^2 + \varepsilon} \right\|_1 \quad (1)$$

The first term is the data fidelity term, where m represents the estimated images, d is the multi-coil pre-interpolated k-space data. W is the undersampling pattern mask, F is the Fourier transform applied to each image frame, S is the coil sensitivity and the multiplication with these matrices equals to the encoding matrix. $\alpha_{xy,t,z}$ represent in-plane spatial, temporal and through-plane spatial regularization weights for spatial, temporal and slice TV constraints respectively. In 3D SoS data reconstruction, α_{xy} = 0.05S, α_t = 0.3S, α_z = 0.02S, where S represents the maximum signal intensity in the first estimated image m. ε is ~10^{-7}. The number of iterations for the reconstruction is chosen as 50 (empirically determined). The equation can also be applied to 2D SMS data if the through-plane spatial TV term is not used and d is pre-interpolated by SMS-GROG and a phase modulation matrix Φ is added to the encoding matrix [17]. Then the weights for spatial and temporal TV constraints are α_{xy} = 0.002S, α_t = 0.02S, respectively.

2D SMS data required an additional step prior to reconstruction to select the range of rays to use for systole (or diastole or any cardiac phase, though only systole was reconstructed in this work). First, a preliminary sliding-window reconstruction was performed to obtain images with a temporal footprint of 55 msec/frame (24 rays). Such a reconstruction was repeatedly created after sliding by three rays (~7msec). Then we manually identified the most systolic images. The rays corresponding to those systolic images were used to perform the final reconstruction.

The work here only used the 3D data acquired near systole, although if heart rate allowed another 3D dataset was acquired each beat at diastole as in [30].

2.3 Post-processing

To compensate for respiratory motion, both rigid and deformable registration were applied. Rigid registration was performed on both PD images and perfusion images. A coarse mask was manually selected to encompass the whole heart and used as input to the registration step. Then a Fourier-based cross-correlation method was applied to iteratively register neighboring frames [41]. Model-based deformable registration was then applied to perfusion images as in [42]. That is, a series of motion-free synthetic images were first generated from fitting a two-compartment model to the images. The fitted images were essentially motion-free and used as the reference in each frame to register the reconstructed images. For the alternating 2D/3D datasets, registration was done for each sequence separately (neighboring frames were redefined as every other beat).

In an image frame generated by the summation of all perfusion frames, a small region was manually drawn within the blood pool area to obtain AIF signal intensity (SI) curves. Lines were drawn conservatively on the summed image to represent the endo- and epicardial border. The myocardial tissue SI curves were obtained from six equiangular myocardial segments in each slice [43].

2.4 Conversion from signal intensities to [Gd]

T1 values of different time frames were estimated by modeling. A Bloch simulation was used to generate a look-up-table (LUT), which converted the measured signal intensities to T1 values. The ratio between perfusion images and the first PD weighted image was the input to the LUT [44]. The Bloch simulation used the prescribed scan parameters and accounted for the slice profile in each excitation RF pulse. For the 2D SMS acquisitions, the slice profile spanning the five slice thicknesses (3 slices plus gaps) was discretized into 1000 samples in the slice direction and the signal evolution of each sample was simulated. Signal intensities from all 1000 samples were summed to give the signal intensity of a specific slice, assuming equal contribution from each radial line readout, and including the appropriate CAIPIRINHA phase modulation [16] for each ray. For 3D imaging, the magnetization signal was simulated, and an extra k_z encoding step was applied to account for readout of each k_z partition. The k-space signal intensity of each k_z partition was averaged and the unacquired k_z partitions (partial Fourier) were kept zero, and then a Fourier transform was applied along k_z to obtain the image space signal intensity for each slice.

Conversion from T1 values to [Gd] curves was then performed by the following equation.

$$[Gd] = \left(\frac{1}{T1} - \frac{1}{T1_{pre}}\right) R^{-1} \qquad (2)$$

T1 comes from the look-up-table (LUT) calculated from the previous step shown above. $T1_{pre}$ is the pre-contrast T1 where native tissue T1 was used either in the blood or myocardium. R is the T1 relaxivity constant, 3.7 $mmol^{-1}s^{-1}$ for Gadoteridol [45].

PD images were acquired using the same gradient echo sequences without the saturation recovery pulse, so the PD images were not truly independent of T1. Such T1 weighting of PD images has been reported

to have negligible effects on the PD image signal intensity [44]. A Bloch simulation was performed here to verify that the use of the first PD image did not bias the conversion to [Gd].

All quantitative MBF results were then calculated with a two-compartment model and an implicit assumption that the extraction fraction is unity.

2.5 Evaluation of every other beat flow values

After quantification, a difference ratio was calculated between EB group and EOB group, as described in the equation below.

$$Ratio = \frac{\sum_{n=1}^{N}\sum_{reg=1}^{6}\frac{|Flow_{EB}(reg,n) - Flow_{EOB}(reg,n)|}{Flow_{EB}(reg,n)}}{6N} \quad (3)$$

In equation (3), $Flow_{EOB}$ is the estimated flow values in the odd or even EOB group, while $Flow_{EB}$ is in the EB group. Each flow represents one of the six segments of the myocardium from a slice and N is the total number of slices (3 for 2D SMS and 6 for 3D SoS).

2.6 Alternating 2D/3D acquisitions

For these acquisitions, the 2D hybrid radial SMS acquisition and the 3D SoS acquisition were applied in an alternating manner as illustrated in Figure 2.

The 2D SMS and 3D SoS EOB acquisitions used the same parameters as the EB sequences described above. The SRT applied before the 2D SMS acquisition was 20msec as was the SRT for the 2D AIF acquired in the same beat as the 3D SoS acquisition. The SRT applied before the 3D centric readout was 100msec. The reconstruction of 2D SMS and 3D SoS alternating acquisitions each used the same STCR method as given above for the EB data. The regularization weights were also the same as for the EB data. One special circumstance is that flow values were different between 2D SMS and 3D SoS methods due primarily to the AIF differences in two out of four stress datasets. Therefore, a composite AIF was created by combining the AIFs in each beat into a single AIF, after conversion to [Gd]. This AIF was then used with EOB tissue curves interpolated to the same temporal resolution in the four stress studies. Though not displayed in this paper, using a composite AIF for the resting cases caused negligible effects on the quantification.

A 9-vial phantom developed for T1 mapping and ECV standardization (T1MES) [46] was used to validate T1 estimates from the alternating 2D/3D sequence. All of the time frames were averaged. The same conversion method using a LUT as described above was used to estimate T1 values in each vial.

Alternating 2D/3D scans were done in 7 dogs (rest: n=10, adenosine stress: n=4) and 2 human subjects (male, age 73, 69 years; rest: n=2) with 0.05-0.075mmol/kg gadoteridol. The adenosine induced stress cases were performed in four dogs with ~280 microgram/kg/min. Another human study was also performed but the ECG triggering was poor, so that dataset was not used. A quantitative perfusion

analysis of absolute MBF for each scan and MPR for the subjects with stress scans was performed followed by Bland-Altman and linear regression. Pearson's correlation coefficient was used to calculate the region-wise relationship between 2D SMS and 3D SoS methods.

3. Results

3.1 Effects of every other beat acquisition on the AIF and myocardium

Figure 3 shows the flow ratio difference (from equation (3)) between EB and EOB data. These results are from two 2D SMS EB data and two 3D SoS EB data.

When using the "ideal" scenario described in the methods above where EOB data was created after EB reconstruction and processing, very low errors were observed between the EB and the EOB group. 2D SMS EOB data showed an average of ~7% estimation error and 3D EOB data showed an average of ~5% estimation error.

In the practical case, when EOB data was reconstructed and processed separately, higher errors were found. 2D SMS EOB data showed an average of ~12% flow ratio difference and 3D EOB data showed an average of ~10% difference.

3.2 Simulation and phantom validation

The PD image signal intensity changes caused by the short TR were investigated with a Bloch equation simulation. The PD images had T1 weighting effects that were <1% variation in the 3D tissue and 2% variation in the 2D SMS tissue when [Gd] was within 0-2 mmol/L. As for the AIF, where [Gd] was typically 0-10 mmol/L, both 2D SMS and 3D had <1% variation. Thus, the T1 weighting of PD images did not bias the conversion to [Gd].

Figure 4 shows measured and reference T1 values in the phantom for the 2D SMS and 3D SoS acquisitions. The top two plots show the T1 estimates using 2D SMS data. The top left displays a linear fit with slope = 1.03 of all nine vials using the first 24 rays of 2D SMS data, while the top right displays a linear fit with slope = 1.00 of all nine vials using ray 40-63. The bottom two plots show the T1 estimates for 3D data. The bottom left displays a linear fit with slope = 1.00 of eight vials using a single slice AIF for 3D, while the bottom right displays a linear fit with slope = 0.98 of eight vials using 3D SoS data. The mean T1 estimations in each plot indicated that errors were <10% for the vials used in the linear fit. The vial with the longest T1 value (1872msec) was biased >10% from the reference in 3D data, though the 3D readout is only used for tissue curves which have shorter T1 even pre-contrast.

3.3 Images with 2D/3D alternating acquisition

The Supporting Information Video S1 shows a time series of all three slices of 2D SMS and all six slices of the corresponding 3D SoS acquisition. The absolute intensities for the three 2D slices was scaled by a

global scale factor to make the contrast of the two movies similar.

3.4 AIF and Tissue [Gd] Curves

Figure 5 shows the comparison of AIFs for 2D SMS and 3D SoS in each dataset. The high similarity between the two AIFs in each subplot indicates that EOB beat acquisition in general does not miss the AIF peak or create significant quantification error.

Figure 6 shows the average tissue [Gd] curves of all myocardial regions and all the slices acquired with 2D SMS and 3D SoS method in each study. The two methods give very similar average tissue [Gd] curves.

3.5 MBF results

Table 2 displays the comparison of MBF results with the alternating 2D SMS and 3D SoS acquisitions. 12 rest scans (10 in dogs and 2 in humans) and 4 stress scans (all in dogs) were included in the analysis. MBF mean and standard deviation in each injection were calculated using all the regions and slices described in the method above and listed in the table. In general, the 2D SMS mean MBF values (rest: 0.68 ± 0.15 ml/g/min; stress: 1.28 ± 0.22 ml/g/min) were comparable to that of 3D (rest: 0.69 ± 0.15 ml/g/min, p=0.85 vs 2D SMS; stress: 1.30 ± 0.24 ml/g/min, p=0.66 vs 2D SMS). The myocardial perfusion reserve calculated using those four dog studies with stress acquisitions were 2.18 ± 0.59 and 2.19 ± 0.53 for 2D SMS and 3D SoS respectively.

Table 2
MBF in 2D SMS and 3D SoS alternating beats

Subject ID	First Injection		Second Injection	
	2D SMS	3D SoS	2D SMS	3D SoS
Dog 1	0.66 ± 0.08	0.74 ± 0.06	0.69 ± 0.09	0.82 ± 0.12
Dog 2	0.79 ± 0.07	0.82 ± 0.10	0.58 ± 0.04	0.63 ± 0.06
Dog 3	0.79 ± 0.19	0.74 ± 0.24	0.83 ± 0.11	0.81 ± 0.09
Dog 4	1.35 ± 0.23	1.42 ± 0.31	0.65 ± 0.06	0.61 ± 0.10
Dog 5	1.07 ± 0.18	1.20 ± 0.17	0.73 ± 0.07	0.72 ± 0.13
Dog 6	1.29 ± 0.17	1.29 ± 0.18	0.49 ± 0.07	0.50 ± 0.06
Dog 7	1.40 ± 0.17	1.29 ± 0.23	0.64 ± 0.04	0.63 ± 0.07
Human 1	0.56 ± 0.14	0.56 ± 0.15		
Human 2	0.75 ± 0.11	0.74 ± 0.08		

(The MBF calculated for each study was the average of three slices and six evenly spaced regions of each slice for 2D SMS and the average of six slices and the same six regions for 3D SoS. The red numbers represent the stress MBF and other cases are rest.)

Figure 7 shows a 2D SMS and 3D SoS MBF comparison in a dog study using a bulls-eye plot including both the rest and the stress perfusion results.

Figure 8 shows the Bland-Altman analysis of the 2D SMS and 3D averaged-slice region-wise flow comparison with r = 0.83 (y = 0.92*x+0.08) and confidence interval (mean difference ± 1.96 standard deviation: [-0.37, 0.35]).

4. Discussion

We proposed a new approach to myocardial perfusion imaging in this study by alternating quantitative radial 2D SMS with a hybrid saturation recovery/gradient echo approach to steady state, and 3D SoS with saturation recovery and preceded by a 2D short SRT AIF each heartbeat. This approach enabled a direct comparison of the 2D SMS and 3D SoS methods with the same gadolinium injection. This approach using these two very different sequences may also help to give a more comprehensive and robust clinical assessment, since artifacts are expected to differ while quantification results are expected from the initial experience here to share similar in-plane distributions. This work also helps to understand the temporal sampling requirements of dynamic contrast-enhanced myocardial perfusion imaging, and enables the creation of more diverse but still quantitative sequences since the tissue curves likely do not need to be sampled EB. Initial results here show this with free-breathing acquisitions, and breath-hold acquisitions likely work better for EOB sequences. As well, dark rim artifacts were not observed with either method used here. This work was to establish technical feasibility, and future work to evaluate these possible advantages in a patient population is needed.

One objective in this paper was to investigate the feasibility of EOB quantification. Previous research reported a semiquantitative evaluation of the effect on the varying sampling rates. That study used a myocardial perfusion reserve index (MPRI) calculated by dividing the upslopes of the time-intensity curves at stress and rest [47]. The resulting MPRI values between EB and EOB were similar when the upslope of the blood and myocardium signal intensity curves in the left ventricle had ~20% difference for both the rest and the stress. In this study, we found that the absolute MBF differences between EB and EOB data can be ~5% higher for both the 2D SMS and 3D SoS data when reconstruction and processing were done separately as mentioned in the results part.

B1 inhomogeneity may cause inaccuracies in estimated T1 and [Gd] values and so affects MBF. Flip angle variations on the order of 30% across the myocardium have been reported in previous research [48–50]. B1 inhomogeneity may cause inaccuracies in estimated T1 and [Gd] values and so affects MBF. Flip angle variations on the order of 30% across the myocardium have been reported in previous research [48–50]. To gauge the degree of B1 biases on the MBF, a flip angle error of 15% was applied in three dogs and one human study. Myocardial signal intensity curves of PD images and T1-weighted images for the AIF and tissue were converted to [Gd] using the biased flip angle. The concentration curves were then fit to the compartment model to give biased MBFs. All of the slices and regions were used to calculate the MBF percent change due to the biased flip angle. When using a prescribed 12° flip angle, if there is a 15%

flip angle reduction to 10.2°, then the MBF was changed in these datasets by 10 ± 5% for 2D SMS data and 4 ± 3% for 3D SoS data.

The accuracy of the AIF is important when quantifying perfusion CMR. Though AIFs for 2D SMS and 3D SoS were similar as displayed in Figure 5, two stress studies showed quantitative perfusion differences of up to 35%, possibly due to the AIFs from the EOB acquisitions. Using a composite AIF by combining the 2D SMS AIF and the 2D AIF from 3D SoS acquisition resulted in very similar 2D SMS and 3D SoS results. Therefore, the four stress cases were processed with a composite AIF (results in Figures 6-8).

Perfusion results can be dependent on the model used. Both two-compartment model and Fermi model were applied to these datasets. The perfusion estimates were similar at rest but different at stress (details in Supporting Information Table S2). This finding is similar to previous studies [51–54]. Compared to published perfusion estimates (resting values ranging from 0.52 ml/min/g to 1.2 ml/min/g and stress values ranging from 1.36 ml/min/g to 4 ml/min/g), perfusion results of this study were generally towards the lower end. This is possibly due to the anesthesia used in the dog studies, lack of extraction fraction corrections.

Respiratory and cardiac motion challenge the quantitative analysis of standard perfusion data. Switching to an EOB sequence can make obtaining good image quality more challenging. Nevertheless, the results here found changes similar to those seen in repeated scan variability [55–59]. Specifically, EOB would lead to ~15% difference in the segmental MBF in practice mentioned above, which is similar to the reported ~20% coefficient of variance in the segmental MBF between two repeated scans [59]. We note that the tissue curves here were mainly from canine studies (n=7), which have relatively small heart movement with respiration.

5. Conclusion

We demonstrated that an alternating quantitative 2D/3D myocardial first-pass perfusion imaging sequence is feasible. The alternating acquisition results in small effects on the accuracy of both AIF and tissue estimation. Though limited by motion effects to some extent, 2D SMS and 3D SoS quantitative results showed a close relationship, with MBF differences within 15%. Further work is needed to understand the trade-offs of the 2D SMS and 3D SoS sequences and the possible complementary information that they may provide.

Declarations

6. Acknowledgement

Research reported in this publication was supported by The National Heart, Lung, and blood Institute of the National Institute of Health under award R01 HL 135328. The content is solely the responsibility of the authors and does not necessarily represent the official views of the National Institute of Health.

Conflict of Interest

The authors declare that they have no conflict of interest.

Footnotes

Ethics approval and consent to participate

The University of Utah Institutional Review Board approved the study. Written consent for participation was obtained from all participants.

Consent for publication

Written consent for publication was obtained from all study participants.

Availability of data and material

The datasets analyzed during the current study are available from the corresponding author on reasonable request.

Authors' contributions

QH, YT, JM made significant contributions to the data acquisition, analysis and interpretation, made significant contributions to propose, revise and approved the final manuscript. RR made significant contributions to the data acquisition and interpretation. GA made significant contributions to the conception and design of the study, data acquisition, analysis and interpretation. ED made significant contributions to the conception and design of the study, data acquisition, analysis and interpretation, and critically reviewed and approved the final manuscript. All authors agreed to be accountable for the accuracy and integrity of the work.

References

1. Christian TF, Rettmann DW, Aletras AH, Liao SL, Taylor JL, Balaban RS, Arai AE (2004) Absolute myocardial perfusion in canines measured by using dual-bolus first-pass MR imaging. Radiology 232(3):677–684
2. Yun CH, Tsai JP, Tsai CT, Mok GS, Sun JY, Hung CL, Wu TH, Huang WT, Yang FS, Lee JJ, Cury RC, Fares A, Nshisso LD, Bezerra HG (2015) Qualitative and semi-quantitative evaluation of myocardium perfusion with 3 T stress cardiac MRI. BMC Cardiovasc Disord 15:164
3. Mordini FE, Haddad T, Hsu LY, Kellman P, Lowrey TB, Aletras AH, Bandettini WP, Arai AE (2014) Diagnostic accuracy of stress perfusion CMR in comparison with quantitative coronary angiography: fully quantitative, semiquantitative, and qualitative assessment. JACC Cardiovasc Imaging 7(1):14–22

4. Hsu LY, Jacobs M, Benovoy M, Ta AD, Conn HM, Winkler S, Greve AM, Chen MY, Shanbhag SM, Bandettini WP, Arai AE (2018) Diagnostic Performance of Fully Automated Pixel-Wise Quantitative Myocardial Perfusion Imaging by Cardiovascular Magnetic Resonance. JACC Cardiovasc Imaging 11(5):697–707
5. Knott KD, Camaioni C, Ramasamy A, Augusto JA, Bhuva AN, Xue H, Manisty C, Hughes RK, Brown LAE, Amersey R, Bourantas C, Kellman P, Plein S, Moon JC (2019) Quantitative myocardial perfusion in coronary artery disease: A perfusion mapping study. J Magn Reson Imaging 50(3):756–762
6. Shin T, Hu HH, Pohost GM, Nayak KS (2008) Three dimensional first-pass myocardial perfusion imaging at 3T: feasibility study,Journal of Cardiovascular Magnetic Resonance10
7. Barth M, Breuer F, Koopmans PJ, Norris DG, Poser BA (2016) Simultaneous multislice (SMS) imaging techniques. Magn Reson Med 75(1):63–81
8. Fair MJ, Gatehouse PD, DiBella EVR, Firmin DN (2015) A review of 3D first-pass, whole-heart, myocardial perfusion cardiovascular magnetic resonance,Journal of Cardiovascular Magnetic Resonance17
9. Sodickson DK, Manning WJ (1997) Simultaneous acquisition of spatial harmonics (SMASH): fast imaging with radiofrequency coil arrays. Magn Reson Med 38(4):591–603
10. Pruessmann KP, Weiger M, Scheidegger MB, Boesiger P (1999) SENSE: sensitivity encoding for fast MRI. Magn Reson Med 42(5):952–962
11. Larkman DJ, Hajnal JV, Herlihy AH, Coutts GA, Young IR, Ehnholm G (2001) Use of multicoil arrays for separation of signal from multiple slices simultaneously excited. J Magn Reson Imaging 13(2):313–317
12. Griswold MA, Jakob PM, Heidemann RM, Nittka M, Jellus V, Wang J, Kiefer B, Haase A (2002) Generalized autocalibrating partially parallel acquisitions (GRAPPA). Magn Reson Med 47(6):1202–1210
13. Breuer FA, Blaimer M, Heidemann RM, Mueller MF, Griswold MA, Jakob PM (2005) Controlled aliasing in parallel imaging results in higher acceleration (CAIPIRINHA) for multi-slice imaging. Magn Reson Med 53(3):684–691
14. Yutzy SR, Seiberlich N, Duerk JL, Griswold MA (2011) Improvements in Multislice Parallel Imaging Using Radial CAIPIRINHA. Magn Reson Med 65(6):1630–1637
15. Nazir MS, Neji R, Speier P, Reid F, Stäb D, Schmidt M, Forman C, Razavi R, Plein S, Ismail TF (2018) Simultaneous multi slice (SMS) balanced steady state free precession first-pass myocardial perfusion cardiovascular magnetic resonance with iterative reconstruction at 1.5 T. J Cardiovasc Magn Reson 20(1):1–11
16. Wang HN, Adluru G, Chen LY, Kholmovski EG, Bangerter NK, DiBella EVR (2016) Radial simultaneous multi-slice CAIPI for ungated myocardial perfusion. Magn Reson Imaging 34(9):1329–1336
17. Tian Y, Mendes J, Pedgaonkar A, Ibrahim M, Jensen L, Schroeder JD, Wilson B, DiBella EVR, Adluru G (2019) Feasibility of multiple-view myocardial perfusion MRI using radial simultaneous multi-slice acquisitions. PLoS ONE 14(2):e0211738

18. Yang Y, Meyer CH, Epstein FH, Kramer CM, Salerno M (2019) Whole-heart spiral simultaneous multi-slice first-pass myocardial perfusion imaging. Magn Reson Med 81(2):852–862
19. Tian Y, Mendes J, Wilson B, Ross A, Ranjan R, DiBella E, Adluru G (2020) Whole-heart, ungated, free-breathing, cardiac-phase-resolved myocardial perfusion MRI by using Continuous Radial Interleaved simultaneous Multi-slice acquisitions at sPoiled steady-state (CRIMP), Magnetic Resonance in Medicine
20. Nazir MS, Neji R, Speier P, Staeb D, Schmidt M, Forman C, Razavi R, Plein S, Ismail T, Roujol S (2018) Feasibility of absolute myocardial blood flow quantification using Simultaneous Multi Slice (SMS) SSFP first-pass myocardial perfusion imaging and iterative reconstruction at 1.5 Tesla, Proc. Intern. Soc. Magn. Reson. Med.(ISMRM),
21. Pedersen H, Kozerke S, Ringgaard S, Nehrke K (2009) Kim, k-t PCA: Temporally Constrained k-t BLAST Reconstruction Using Principal Component Analysis. Magn Reson Med 62(3):706–716
22. Vitanis V, Manka R, Boesiger P, Kozerke S (2009) Accelerated Cardiac Perfusion Imaging Using k-t SENSE with SENSE Training. Magn Reson Med 62(4):955–965
23. Otazo R, Kim D, Axel L, Sodickson DK (2010) Combination of Compressed Sensing and Parallel Imaging for Highly Accelerated First-Pass Cardiac Perfusion MRI. Magn Reson Med 64(3):767–776
24. Iyer SK, Tasdizen T, Likhite D, DiBella E (2016) Split Bregman multicoil accelerated reconstruction technique: A new framework for rapid reconstruction of cardiac perfusion MRI. Med Phys 43(4):1969–1981
25. Manka R, Jahnke C, Kozerke S, Vitanis V, Crelier G, Gebker R, Schnackenburg B, Boesiger P, Fleck E, Paetsch I (2011) Dynamic 3-Dimensional Stress Cardiac Magnetic Resonance Perfusion Imaging Detection of Coronary Artery Disease and Volumetry of Myocardial Hypoenhancement Before and After Coronary Stenting. J Am Coll Cardiol 57(4):437–444
26. Vitanis V, Manka R, Giese D, Pedersen H, Plein S, Boesiger P, Kozerke S (2011) High Resolution Three-Dimensional Cardiac Perfusion Imaging Using Compartment-Based k-t Principal Component Analysis. Magn Reson Med 65(2):575–587
27. Shin T, Nayak KS, Santos JM, Nishimura DG, Hu BS, McConnell MV (2013) Three-dimensional first-pass myocardial perfusion MRI using a stack-of-spirals acquisition. Magn Reson Med 69(3):839–844
28. Motwani M, Kidambi A, Sourbron S, Fairbairn TA, Uddin A, Kozerke S, Greenwood JP, Plein S (2014) Quantitative three-dimensional cardiovascular magnetic resonance myocardial perfusion imaging in systole and diastole. J Cardiovasc Magn Reson 16:19
29. Manka R, Paetsch I, Kozerke S, Moccetti M, Hoffmann R, Schroeder J, Reith S, Schnackenburg B, Gaemperli O, Wissmann L, Wyss CA, Kaufmann PA, Corti R, Boesiger P, Marx N, Luscher TF, Jahnke C (2012) Whole-heart dynamic three-dimensional magnetic resonance perfusion imaging for the detection of coronary artery disease defined by fractional flow reserve: determination of volumetric myocardial ischaemic burden and coronary lesion location. Eur Heart J 33(16):2016–2024

30. Mendes JK, Adluru G, Likhite D, Fair MJ, Gatehouse PD, Tian Y, Pedgaonkar A, Wilson B, DiBella EVR (2020) Quantitative 3D myocardial perfusion with an efficient arterial input function. Magn Reson Med 83(6):1949–1963
31. Huber A, Sourbron S, Klauss V, Schaefer J, Bauner KU, Schweyer M, Reiser M, Rummeny E, Rieber J (2012) Magnetic Resonance Perfusion of the Myocardium Semiquantitative and Quantitative Evaluation in Comparison With Coronary Angiography and Fractional Flow Reserve. Invest Radiol 47(6):332–338
32. Motwani M, Fairbairn TA, Larghat A, Mather AN, Biglands JD, Radjenovic A, Greenwood JP, Plein S (2012) Systolic versus Diastolic Acquisition in Myocardial Perfusion MR Imaging. Radiology 262(3):816–823
33. Coelho-Filho OR, Rickers C, Kwong RY, Jerosch-Herold M (2013) MR myocardial perfusion imaging. Radiology 266(3):701–715
34. Motwani M, Jogiya R, Kozerke S, Greenwood JP, Plein S (2013) Advanced cardiovascular magnetic resonance myocardial perfusion imaging: high-spatial resolution versus 3-dimensional whole-heart coverage. Circ Cardiovasc Imaging 6(2):339–348
35. Wissmann L, Gotschy A, Santelli C, Tezcan KC, Hamada S, Manka R, Kozerke S (2017) Analysis of spatiotemporal fidelity in quantitative 3D first-pass perfusion cardiovascular magnetic resonance. J Cardiovasc Magn Reson 19(1):11
36. Qi Huang YT, Mendes J, Adluru G, DiBella E (2020) Quantitative myocardial perfusion with an alternating radial 2D simultaneous multi-slice and 3D stack-of-stars sequence, Proc. Intern. Soc. Magn. Reson. Med.(ISMRM),
37. Chow K, Kellman P, Spottiswoode BS, Nielles-Vallespin S, Arai AE, Salerno M, Thompson RB (2015) Saturation pulse design for quantitative myocardial T1 mapping. J Cardiovasc Magn Reson 17:84
38. Adluru G, McGann C, Speier P, Kholmovski EG, Shaaban A, DiBella EVR (2009) Acquisition and Reconstruction of Undersampled Radial Data for Myocardial Perfusion Magnetic Resonance Imaging. J Magn Reson Imaging 29(2):466–473
39. Chen LY, Adluru G, Schabel MC, McGann CJ, DiBella EVR (2012) Myocardial perfusion MRI with an undersampled 3D stack-of-stars sequence. Med Phys 39(8):5204–5211
40. Tian Y, Erb KC, Adluru G, Likhite D, Pedgaonkar A, Blatt M, Kamesh Iyer S, Roberts J, DiBella E (2017) Technical Note: Evaluation of pre-reconstruction interpolation methods for iterative reconstruction of radial k-space data, Med Phys 44(8) 4025-4034
41. Ge P, Lan CY, Wang H (2014) An improvement of image registration based on phase correlation. Optik 125(22):6709–6712
42. Adluru G, DiBella EVR, Schabel MC (2006) Model-based registration for dynamic cardiac perfusion MRI. J Magn Reson Imaging 24(5):1062–1070
43. Cerqueira MD, Weissman NJ, Dilsizian V, Jacobs AK, Kaul S, Laskey WK, Pennell DJ, Rumberger JA, Ryan T, Verani MS (2002) American Heart Association Writing Group on Myocardial, I. Registration for Cardiac, Standardized myocardial segmentation and nomenclature for tomographic imaging of

the heart. A statement for healthcare professionals from the Cardiac Imaging Committee of the Council on Clinical Cardiology of the American Heart Association. Int J Cardiovasc Imaging 18(1):539–542

44. Kellman P, Hansen MS, Nielles-Vallespin S, Nickander J, Themudo R, Ugander M, Xue H (2017) Myocardial perfusion cardiovascular magnetic resonance: optimized dual sequence and reconstruction for quantification,Journal of Cardiovascular Magnetic Resonance19
45. Blockley NP, Jiang L, Gardener AG, Ludman CN, Francis ST, Gowland PA (2008) Field strength dependence of R1 and R2* relaxivities of human whole blood to ProHance, Vasovist, and deoxyhemoglobin. Magn Reson Med 60(6):1313–1320
46. Captur G, Gatehouse P, Keenan KE, Heslinga FG, Bruehl R, Prothmann M, Graves MJ, Eames RJ, Torlasco C, Benedetti G, Donovan J, Ittermann B, Boubertakh R, Bathgate A, Royet C, Pang WJ, Nezafat R, Salerno M, Kellman P, Moon JC (2016) A medical device-grade T1 and ECV phantom for global T1 mapping quality assurance-the T-1 Mapping and ECV Standardization in cardiovascular magnetic resonance (T1MES) program,Journal of Cardiovascular Magnetic Resonance18
47. Thiele H, Plein S, Ridgway JP, Breeuwer M, Higgins D, Schuler G, Sivananthan M (2003) Effects of missing dynamic images on myocardial perfusion reserve index calculation: Comparison between an every heartbeat and an alternate heartbeat acquisition. J Cardiovasc Magn Reson 5(2):343–352
48. Sung K, Nayak KS (2008) Measurement and characterization of RF nonuniformity over the heart at 3T using body coil transmission. J Magn Reson Imaging 27(3):643–648
49. Schar M, Vonken EJ, Stuber M (2010) Simultaneous B(0)- and B(1)+-map acquisition for fast localized shim, frequency, and RF power determination in the heart at 3 T. Magn Reson Med 63(2):419–426
50. Weingartner S, Zimmer F, Metzger GJ, Ugurbil K, Van de Moortele PF, Akcakaya M (2017) Motion-robust cardiac B1+ mapping at 3T using interleaved bloch-siegert shifts. Magn Reson Med 78(2):670–677
51. Pack NA, DiBella EV (2010) Comparison of myocardial perfusion estimates from dynamic contrast-enhanced magnetic resonance imaging with four quantitative analysis methods. Magn Reson Med 64(1):125–137
52. Ritter C, Brackertz A, Sandstede J, Beer M, Hahn D, Kostler H (2006) Absolute quantification of myocardial perfusion under adenosine stress. Magn Reson Med 56(4):844–849
53. Fritz-Hansen T, Hove JD, Kofoed KF, Kelbaek H, Larsson HB (2008) Quantification of MRI measured myocardial perfusion reserve in healthy humans: a comparison with positron emission tomography. J Magn Reson Imaging 27(4):818–824
54. Utz W, Greiser A, Niendorf T, Dietz R, Schulz-Menger J (2008) Single- or dual-bolus approach for the assessment of myocardial perfusion reserve in quantitative MR perfusion imaging. Magn Reson Med 59(6):1373–1377
55. Elkington AG, Gatehouse PD, Ablitt NA, Yang GZ, Firmin DN, Pennell DJ (2005) Interstudy reproducibility of quantitative perfusion cardiovascular magnetic resonance. J Cardiovasc Magn

Reson 7(5):815–822

56. Jerosch-Herold M, Vazquez G, Wang L, Jacobs DR Jr, Folsom AR (2008) Variability of myocardial blood flow measurements by magnetic resonance imaging in the multi-ethnic study of atherosclerosis. Invest Radiol 43(3):155–161
57. Morton G, Jogiya R, Plein S, Schuster A, Chiribiri A, Nagel E (2012) Quantitative cardiovascular magnetic resonance perfusion imaging: inter-study reproducibility. Eur Heart J Cardiovasc Imaging 13(11):954–960
58. Larghat AM, Maredia N, Biglands J, Greenwood JP, Ball SG, Jerosch-Herold M, Radjenovic A, Plein S (2013) Reproducibility of first-pass cardiovascular magnetic resonance myocardial perfusion. J Magn Reson Imaging 37(4):865–874
59. Likhite D, Suksaranjit P, Adluru G, Hu N, Weng C, Kholmovski E, McGann C, Wilson B, DiBella E (2016) Interstudy repeatability of self-gated quantitative myocardial perfusion MRI. J Magn Reson Imaging 43(6):1369–1378

Figures

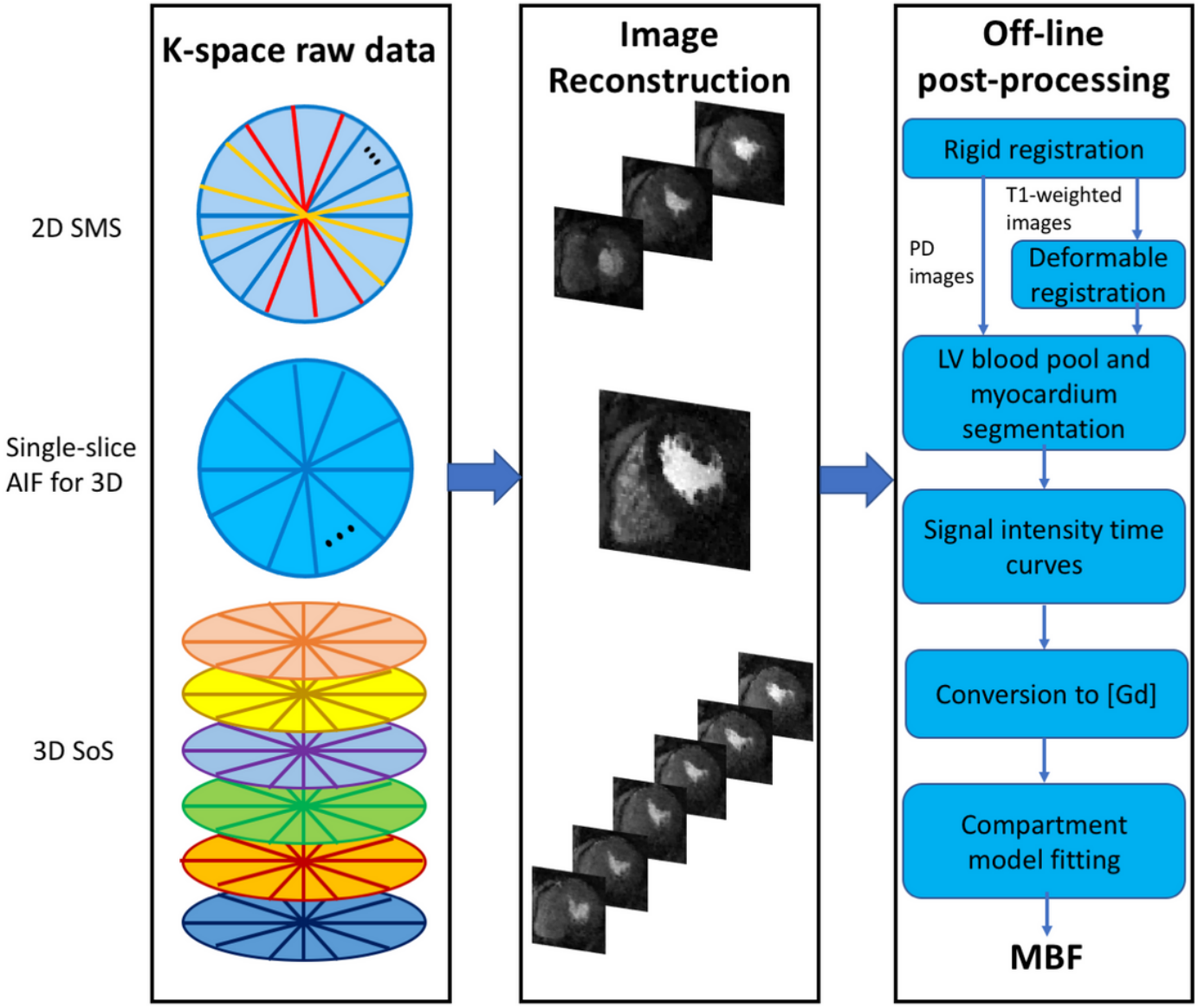

Figure 1

General data processing flowchart. The 2D/3D alternating sequence acquires three sets of k-space raw data. These data can be reconstructed by a spatial-temporal constrained reconstruction algorithm respectively. Then an off-line post-processing pipeline can be used, including registration, signal intensity curves extraction, conversion to [Gd] and model fitting, to obtain quantitative perfusion values. One detail in the figure is that PD images would only require rigid registration due to no obvious contrast change, but T1-weighted images need to be applied in both rigid and deformable registration

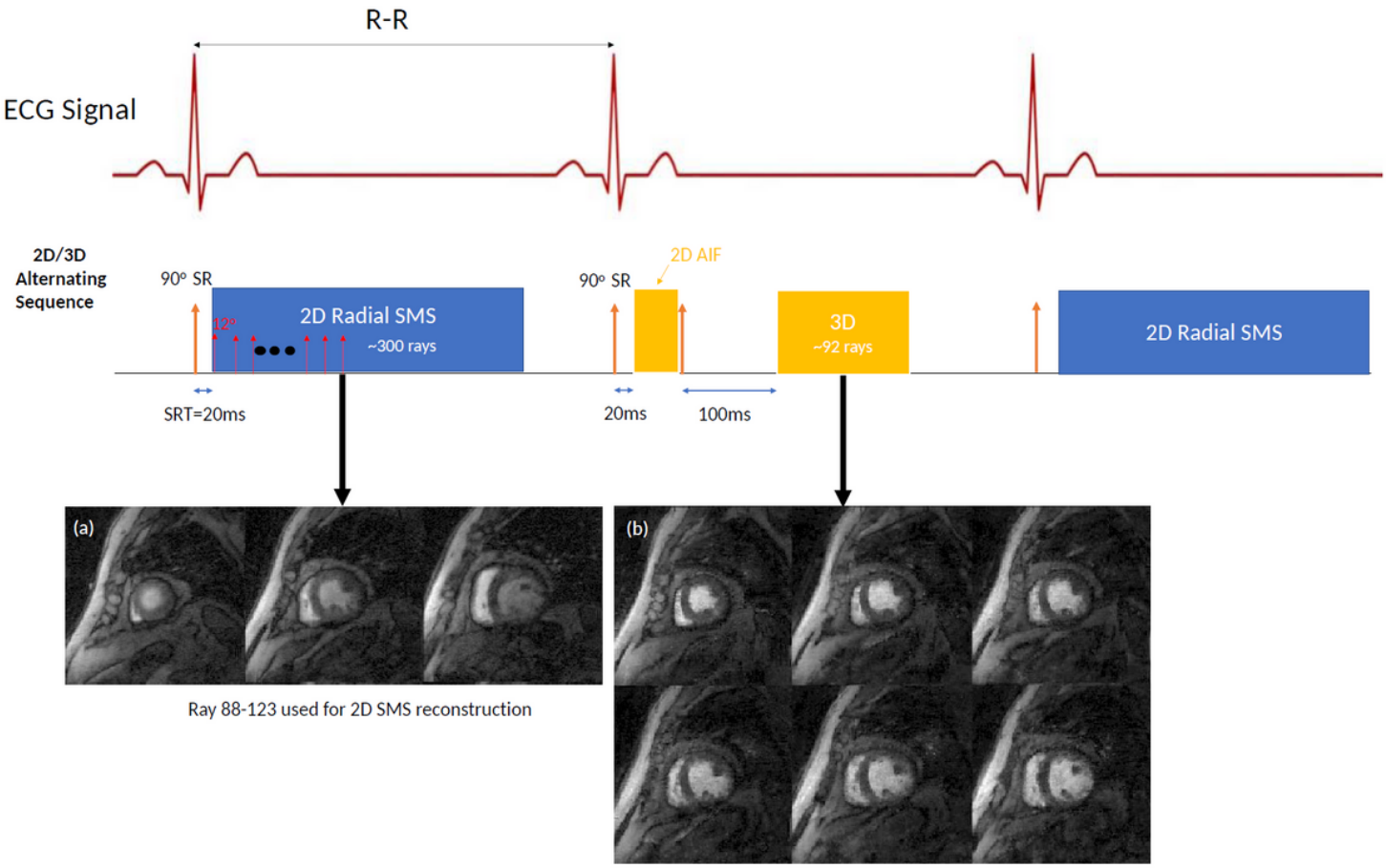

Figure 2

The 2D/3D alternating acquisition. The sequence includes a 90o saturation recovery pulse followed by a 2D FLASH SMS readout or a 3D SoS acquisition with 8 slices every other heartbeat (the two edge slices are not used). The SRT is 20 ms for 2D acquisition and 100 ms for 3D readouts. Gradient echo readouts use a 12o flip angle and a multi-band factor of 3 was applied in the SMS acquisition. An example of 2D SMS (a) and 3D SoS (b) images are displayed

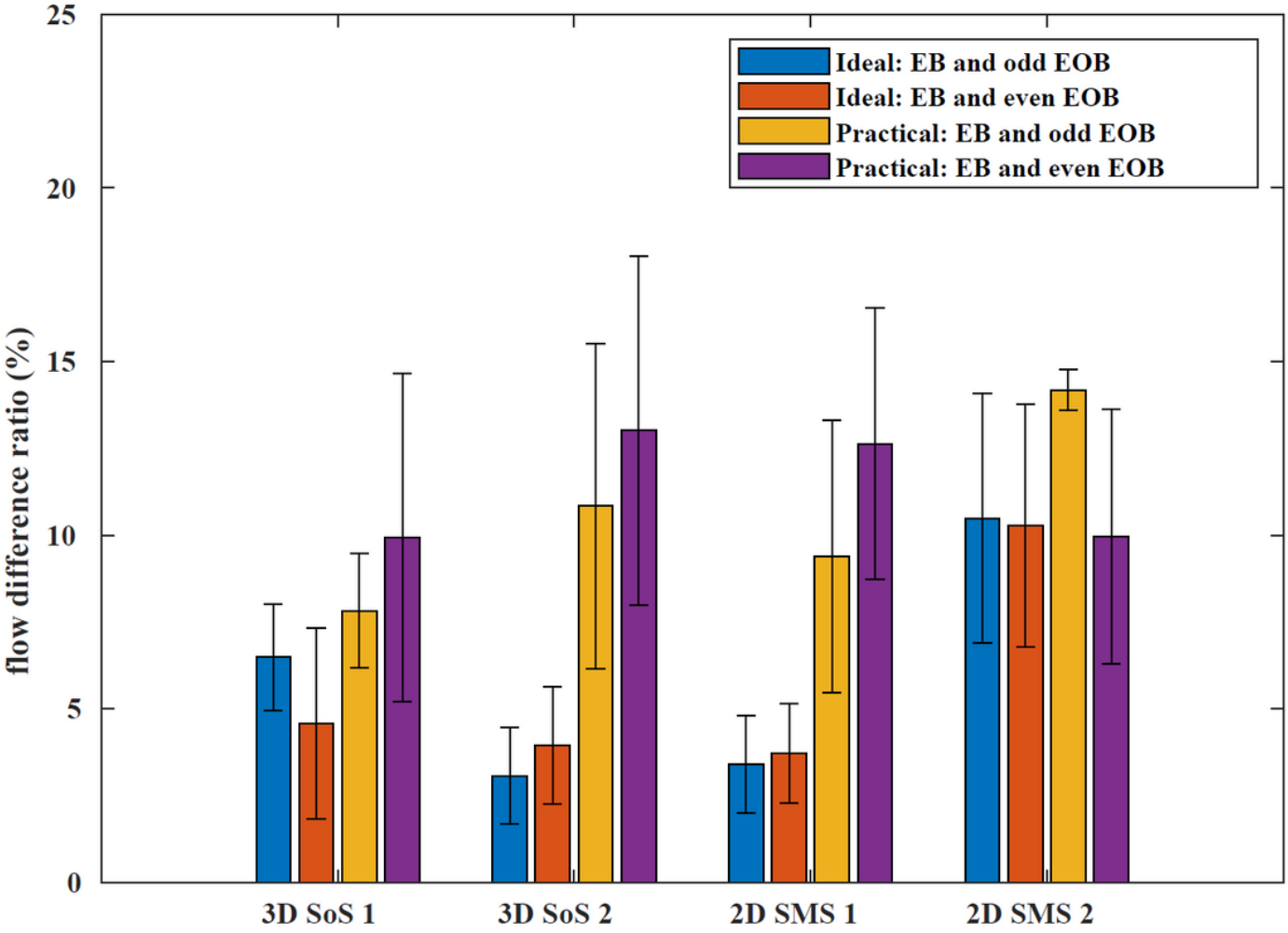

Figure 3

EB and EOB flow ratio difference in ideal and practical processing conditions respectively. The average absolute flow ratio difference based on each region of each slice of a patient is shown using ideal processing (blue and orange bars) and using practical processing (yellow and purple bars)

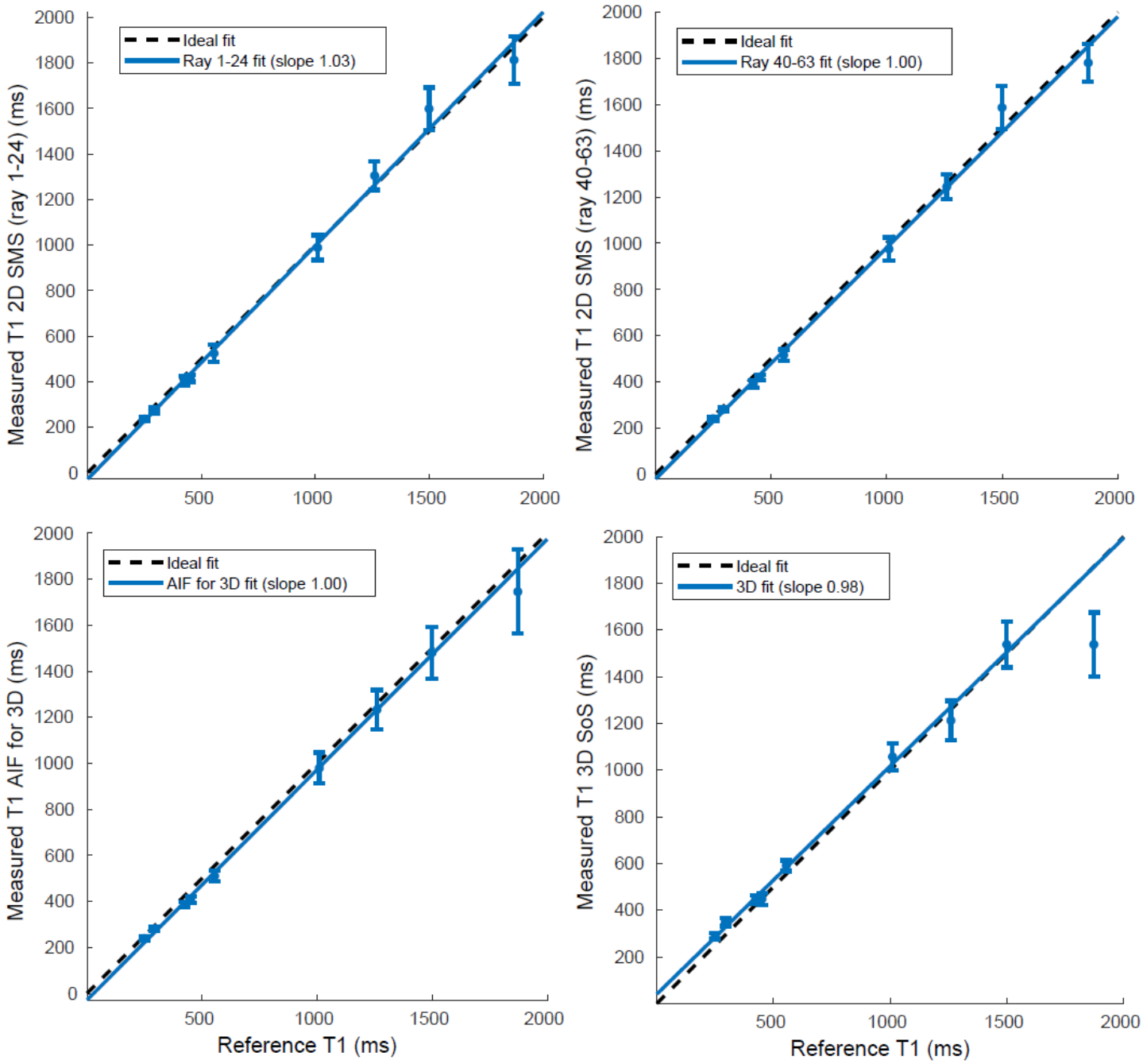

Figure 4

Phantom validation of measured T1 from 2D/3D alternating sequence and reference T1 from MOLLI sequence. The top two plots show the T1 estimates using 2D SMS data. The top left displays the error bars from each vial and a linear fit of all nine vials using first 24 rays of 2D SMS data, while the top right using ray 40-63. The bottom two plots show the T1 estimates for 3D data. The bottom left displays the error bars from each vial and a linear fit of eight vials using a single slice AIF for 3D, while the bottom right using 3D SoS data. The vial with the highest T1 value was biased >10% from the reference in 3D data, thus not used

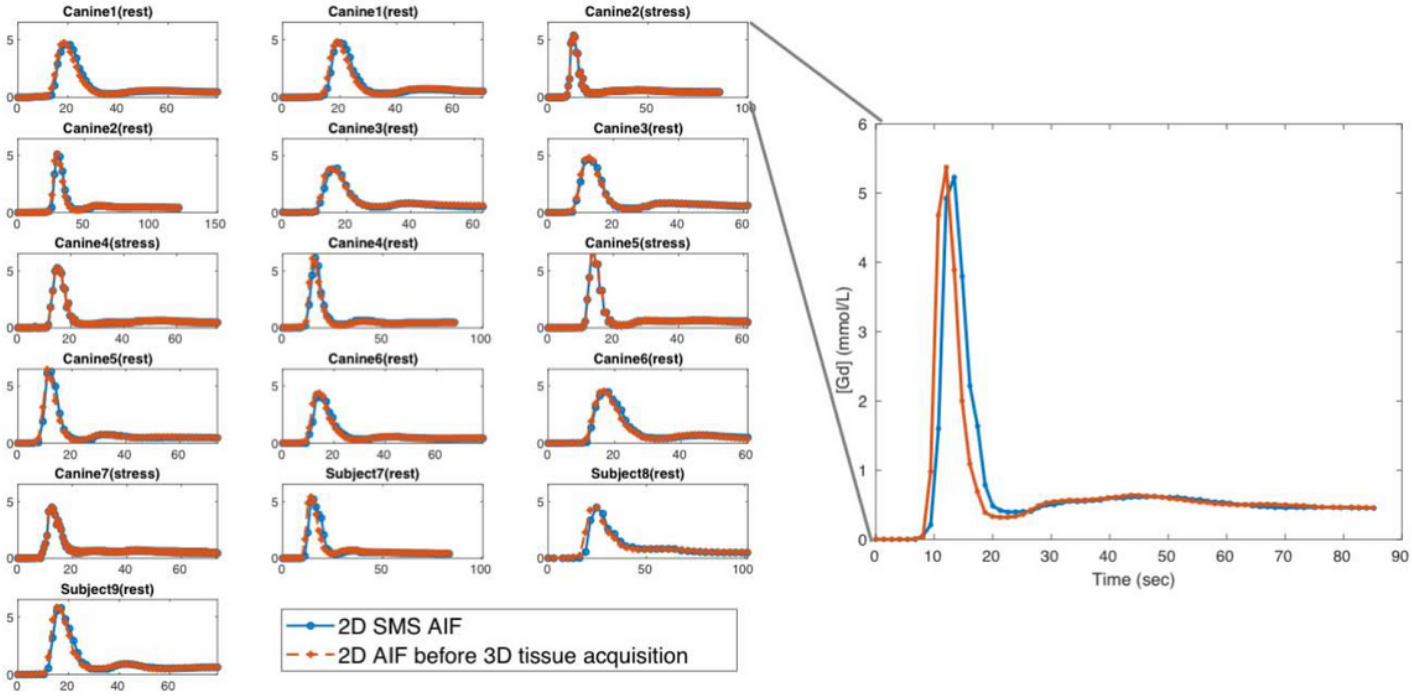

Figure 5

AIF [Gd] curves comparison between 2D SMS and 3D SoS for all in-vivo studies. The orange curves represent the single-slice AIF for 3D SoS while the blue curves show a 2D AIF from a similar SMS slice. Among all of the AIFs shown, the first seven cases were canine studies while the last two were human studies. The right figure shows a zoomed example of one stress case in which MBF differed if a composite AIF was not used

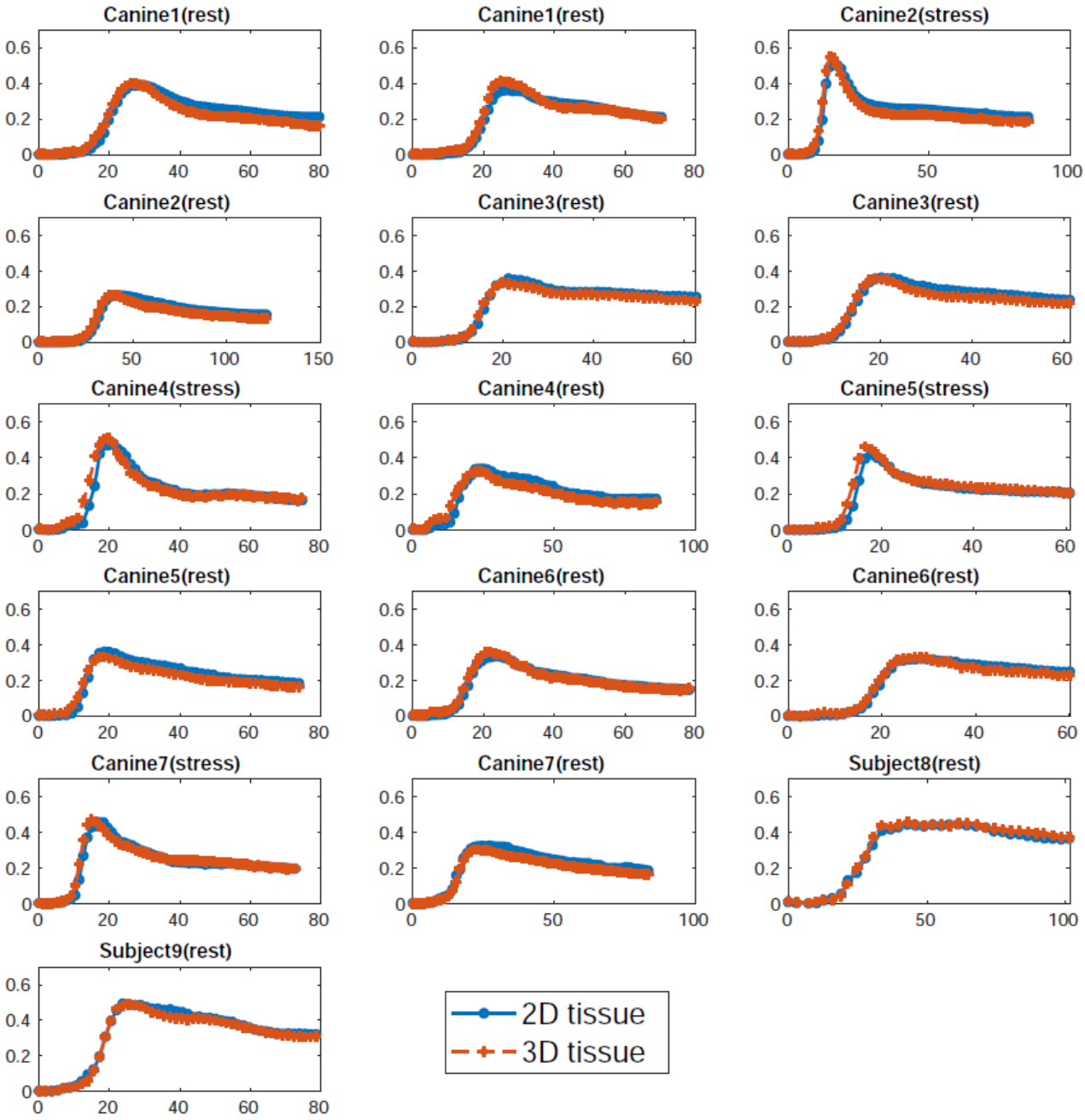

Figure 6

Average tissue [Gd] curves comparison between 2D SMS and 3D in all in-vivo studies. The orange curves represent the mean of six central slices from 3D tissue while the blue curves show the mean of three slices from 2D tissue. Among all subjects shown above, the first 7 cases were canine studies while the last two were human studies. For all subplots in the figure, the vertical axes unit is “mmol/L” and the horizontal axes unit is “sec”

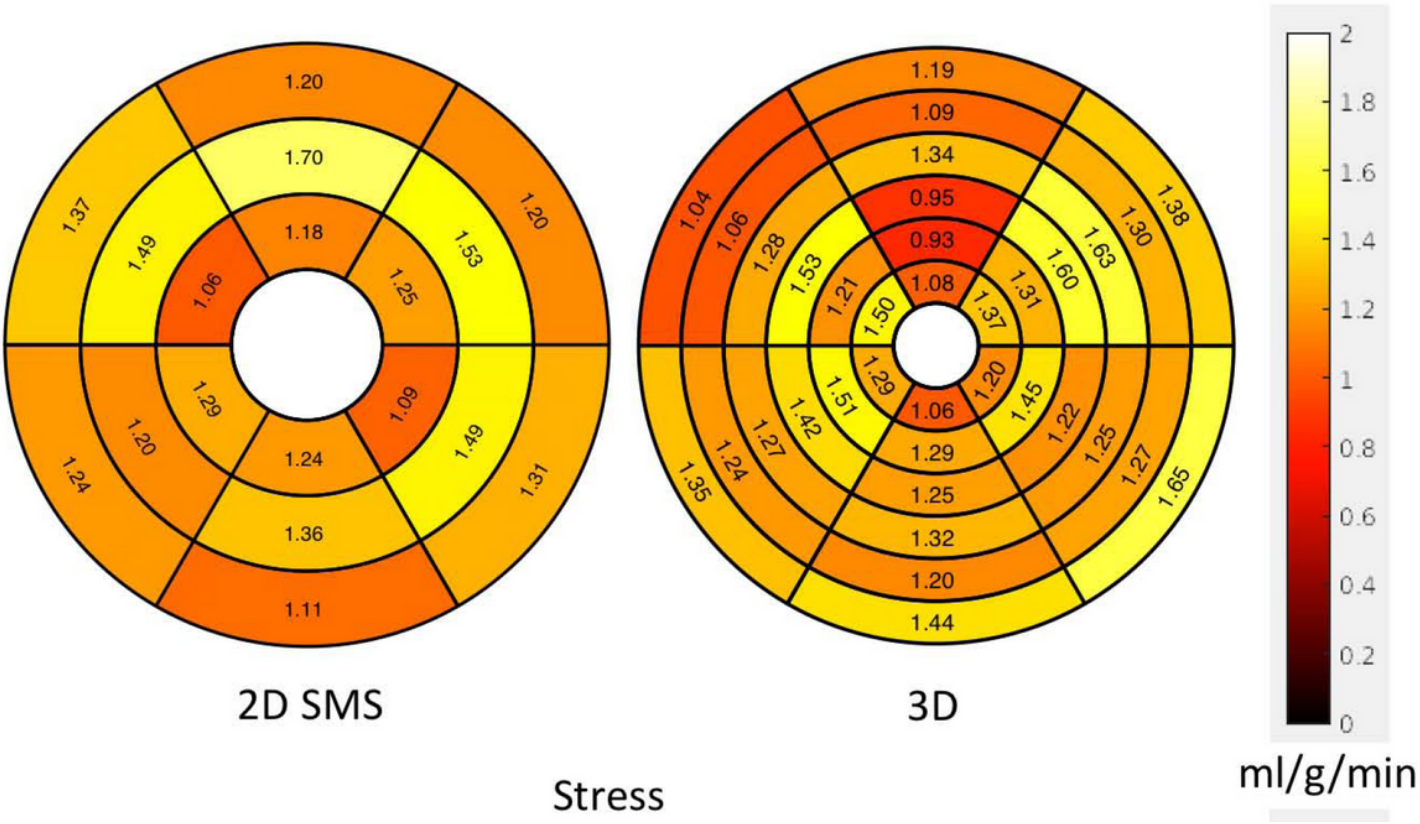

Figure 7

An example of a quantitative perfusion map with 2D SMS and 3D SoS at both rest and stress. The top row shows the comparison at stress while the bottom row shows the rest case. Each 2D SMS acquisition has three slices acquired simultaneously while 3D SoS has six slices. Each slice was divided into six regions by a semi-automatic processing tool

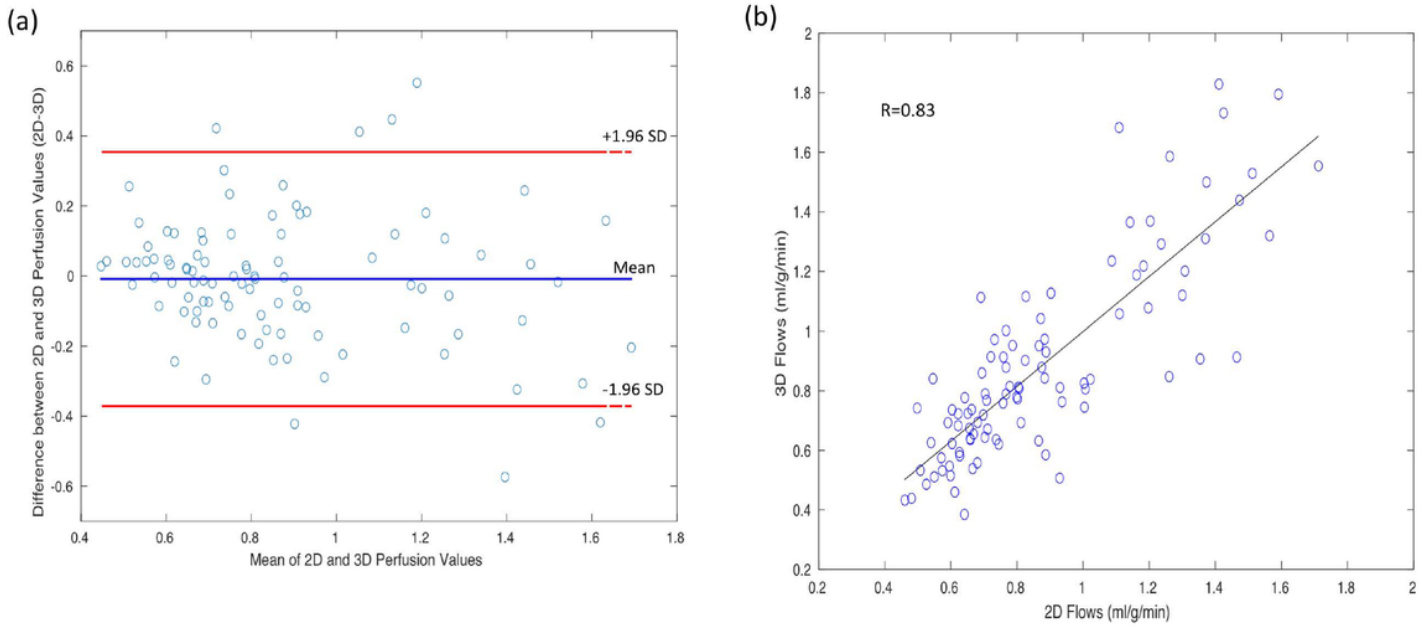

Figure 8

Bland-Altman and correlation analysis of myocardial perfusion. Each point represents a regional flow value. Figure 8(a) shows the average results of all slices. Figure 8(b) shows the correlation plot between 2D SMS and 3D SoS flow values, r = 0.83

Supplementary Files

This is a list of supplementary files associated with this preprint. Click to download.

- SupportingInformation.docx
- SupportingInformationVideoS1.mov